WARWICK
THE UNIVERSITY OF WARWICK

Original citation:
Humphry-Baker, S. A., Marshall, J. M., Smith, G. D. W. and Lee, W. E. (2017) Thermophysical properties of Co-free WC-FeCr hardmetals. In: 19th Plansee Seminar International Journal of Refractory Metals and Hard Materials, Reutte, Austria, 29 May – 2 Jun 2017. Published in: Proceedings of the 19th Plansee Seminar International Journal of Refractory Metals and Hard Materials (In Press)

Permanent WRAP URL:
http://wrap.warwick.ac.uk/94047

warwick.ac.uk/lib-publications

Thermophysical properties of Co-free WC-FeCr hardmetals

S.A. Humphry-Baker*, J.M. Marshall**, G.D.W Smith***, W.E. Lee*

* Department of Materials, Imperial College London, SW7 2BP, UK

** Sandvik Hyperion, CV4 9XG, Coventry, UK

*** Tokamak Energy Ltd., OX14 3DB, Oxfordshire, UK

Abstract

Fe-Cr alloys can potentially replace carcinogenic Co as the binder system in WC-hardmetals. Furthermore, they may be used in emerging applications such as nuclear fusion reactor shielding, where use of Co is forbidden due to the formation of hazardous activated species. In such applications, a good understanding of thermophysical properties is critical to predicting high temperature performance. By combining several thermal analysis techniques (dilatometry, laser flash and calorimetry) we have determined the thermal conductivity and thermal expansivity of several grades of WC-FeCr hardmetals between room temperature and 1200 °C. In these materials the WC grain size was varied between 0.2 and 5 microns. The binder content was kept constant at 10 wt.%, and the nominal binder composition was Fe-8 wt.% Cr. The room temperature thermal conductivities of these materials varied between about 50 and 110 W/m-K, which are similar values to analogous WC-Co materials. Thermal expansion curves exhibited discontinuous shrinkage events at about 850 °C, due to an allotropic phase transition within the FeCr binder between its BCC and FCC structures. The magnitude of the shrinkage was about a third that predicted by the rule-of-mixtures, suggesting significant internal stresses could be generated during the transformation. Such internal stresses could affect the properties of WC-FeCr hardmetals when operating at high temperature.

Keywords

Hardmetals, WC, FeCr, Alternative binders, Thermal conductivity, Thermal expansion

Introduction

Iron-chromium alloys are potential replacements for cobalt alloys in bonding WC-hardmetals. Despite cobalt being the best-known binder material, there has been much interest in finding alternatives due to issues of cost and availability [1, 2]. Recently, this search has gained fresh momentum due to new understanding over the carcinogenic effects of cobalt powder inhalation [3]. By contrast, the Fe-Cr system has a relatively low toxicity and low cost. Furthermore, FeCr-based hardmetals show promise for applications in nuclear fusion reactors [4] due to their low formation rates for hazardous transmutation species under neutron irradiation and their low rates of corrosion compared to conventional WC-Co

hardmetals. Athough the processing and mechanical behavior of hardmetals with Fe-based binders are well understood [5–7], relatively little is known about their thermophysical properties. An improved understanding is required, because problems such as thermal stresses, creep and oxidation can lead to early component failure during high temperature operation. These issues pertain to both conventional wear applications as well as nuclear environments. Thus, accurate thermal expansion and thermal conducitivity data are needed.

WC-based hardmetals have high thermal conductivities. At room temperature, they are typically on the order of 100 W/m-K [8]. Their impressive conductivity is due to the major constituent, WC, which has a high conductivity compared to other non-oxide ceramics. This is partly due to the narrow stoichiometry range and thus low point-defect concentrations exhibited by WC. The conductivity of coarse-grained WC was reported to be 63 [9] and 88 W/m-K [10], however the studied samples were porous and in the fully dense state it is likely much higher. The conductivity of hardmetals decreases with increasing binder content [9–12]. For example, in the WC-Co system, the conducitivty of a 30 wt.% Co allow has about half the conductivity of a 3 wt.% one [9]. This trend is surprising, since Co has a high conductivity of around 100 W/m-K, but can be explained on the basis of the high solubility of W and C in Co, which would drastically lower its conductivity. The effect of WC grain size is less clear: Neumann reported an increase in conductivity with increasing grain size [11, 12], whereas Perecherla and Williams report no trend [9]. Regarding the thermal expansion of WC-Co, there has been little reported, presumably because thermal expansion is relatively insensitive to microstructure; it is reported to be grain size independent [8] and increases only slightly with binder content, since Co has a higher thermal expansion coefficient than WC – about 13 vs 3.4×10^{-6} K^{-1}. Room temperature expansion coefficients are typically $5 - 6 \times 10^{-6}$ [8].

The thermophysical properties of WC-FeCr are necessarily more complex that WC-Co, due to the allotropic BCC-FCC phase transition that occurs in Fe at 910 °C, or about 855 °C in Fe-8 wt.% Cr [13]. This transition invokes both a volumetric shrinkage of about 1 % and an endothermic heat absorption of 1018 J/mol [14]. In this study, we report on the thermal conductivity and thermal expansion behavior of a WC-based hardmetal with a binder of the composition Fe-8 wt.% Cr. This composition was selected as it is close to the Cr-content at which the BCC-FCC phase transition occurs congruently, i.e. at a single temperature. Properties were measured between room temperature and 1200 °C, which is just above the eutectic liquid formation temperature. Overall, the properties compare well with WC-Co hardmetals, which holds promise for their use in thermally-demanding applications.

Experimental

WC-FeCr hardmetals were prepared by mixing WC powders and prealloyed $Fe_{92}Cr_8$ powders in the ratio 90 wt.% WC to 10 wt.% FeCr. Five different samples were prepared, using WC powders of various nominal particle sizes between 0.4 and 8 μm (exact sizes given in Table 2). The median particle diameter for the $Fe_{92}Cr_8$ powders was 7 μm in all cases. Powders were ball-milled with ethanol and an organic binder, dried and pressed using standard laboratory scale powder metallurgy techniques used for simulating industrial production methods [15]. Samples were sintered under vacuum for 1 hour at 1450 °C. On cooling, samples were measured using standard quality control methods to determine shrinkage, density and mass loss.

The as-sintered materials were microstructurally examined as follows: To determine the WC grain size, polished cross sections were imaged in a JSM 6010 Scanning Electron Microscope (SEM) and a LEO Gemini 1525 Field Emission Gun SEM, operated in secondary electron imaging (SEI) mode. WC grain size was estimated using the linear intercept method on at least 100 grains. To quantitatively assess the proportions of each phase present, X-ray Diffraction (XRD) was performed using a PAnalytical X'Pert Powder diffractometer with Cu-source radiation. Diffraction patterns were fitted using the Rietveld refinement technique, using crystallographic information for hexagonal WC (PDF 101-3982), ferritic α-Fe (PDF 1-1267) and the cubic Fe_3W_3C phase (PDF 170-7470). The density of the compacts was determined by the Archimedes method using a Metter Toledo temperature corrected precision balance at 20 °C.

Thermal expansion was measured using a Netzsch 402DIL dilatometer. Cuboidal samples of 4 x 6 x 25 mm were loaded into an alumina pushrod assembly that maintains sample contact through a small compressive force of 75 mN. Samples were heated at 5 K/min to 1200 °C, held for 10 mins, and cooled at the same rate – all in the presence of helium. Instrument thermal expansion was corrected for using an alumina standard. Thermal expansion coefficients were calculated at intervals of 100 °C by averaging the thermal expansion from 50 °C below to 50 °C above the interval. The procedure was performed for both heating and cooling, and the average taken. Thermal diffusivity was measured using a Netzsch LFA 427 laserflash analyser. Disk-shaped samples of 12.7 mm diameter and 3–4 mm thickness were coated with graphite to reduce surface reflectivity. Diffusivity measurements were taken at intervals of 100 °C, with each measurement repeated 3 times at the set-point temperature. All measurements were performed in flowing argon. The laser pulse had a voltage of 600 V and a pulse duration of 0.8 ms. The effect of pulse duration and heat losses were corrected for using the Cowan method [16]. Specific heat capacity measurements were performed using a Netzsch STA 449 F1 Jupiter instrument with dedicated platinum DSC sensor using argon purging gas. The standard ratio method was employed (ISO 11357-4) which consisted of three separate runs: (i) a baseline run; (ii) a run with sapphire standard of 84 mg; and (iii) a run with hardmetal sample of approximately approximately 300 mg. These masses were selected so that the DSC signal intensities of the sample and standard were well matched, both having peak voltages of about 30 μV. In all runs the same platinum crucibles were heated at 20 K/min between 40 and 1200 °C, with 30 minute isothermals before and after the transient.

Results and Discussion

Microstructural characterisation

Table 1 shows the sintering behavior of the 5 samples made in this study. Samples are labelled A-E, corresponding to the nominal particle size classification of the WC powder used. The density, ρ, tended to increase with decreasing WC particle size, from 14.21 g/cm^3 in the finest grained sample to 13.55 g/cm^3 for the coarsest. This is most likely due to the increased driving force for densification in fine-grained materials.

Table 1 also shows the relative densities, which are defined as the percentage of the predicted theoretical density of 14.41 g/cm^3. The relative density, $\rho/\rho*$, varies from about 94 % to 99 %. In general, the densities of WC-FeCr were lower than those of conventional WC-Co materials with the same binder

Table 1:   Sintering characteristics of WC-FeCr.

sample	nominal WC grain size (μm)	density, ρ g cm^{-3}	$\rho/\rho*$ %	3D shrinkage %	mass loss %
A	0.4	14.21	98.6	21.4	3.5
B	0.8	14.06	98.4	17.9	2.2
C	2	13.98	97.8	17.1	2.2
D	6	13.5	94	14.1	3.6
E	8+	13.55	94	15.5	2.2

content. This is partly due to the lower density of the Fe8Cr binder phase (7.85 g cm^{-3}) compared to Co metal (8.89 g cm^{-3}).

Fig. 1 shows typical SEM micrographs of each sample. The WC grain size varies from about 0.2 μm (A) to 5 μm (E). The microstructures are fairly uniform, except for sample A, where pools of binder phase are visible, about 1–5 μm in width, particularly in the upper-right region (denoted by a dashed circle). This is because the FeCr particles were very much larger than WC particles (median size of about 7 μm, vs about 0.2 μm. In all of the samples a third phase is visible that is intermediate in contrast between WC (light) and FeCr (dark). This phase is likely to be the Fe_3W_3C present in the XRD patterns shown in Fig. 2 and is denoted by arrows in the SEM images for samples C and D.

Fig. 2 clearly shows how the quanitity of the Fe_3W_3C phase increases with decreasing WC grain size, with the Fe_3W_3C peaks becoming progressively more intense. Correspondingly, the (110) FeCr peak at 44.6 ° 2θ becomes less intense, which is consistent with Fe_3W_3C being formed as a reaction product between FeCr and WC during the liquid phase sintering process.
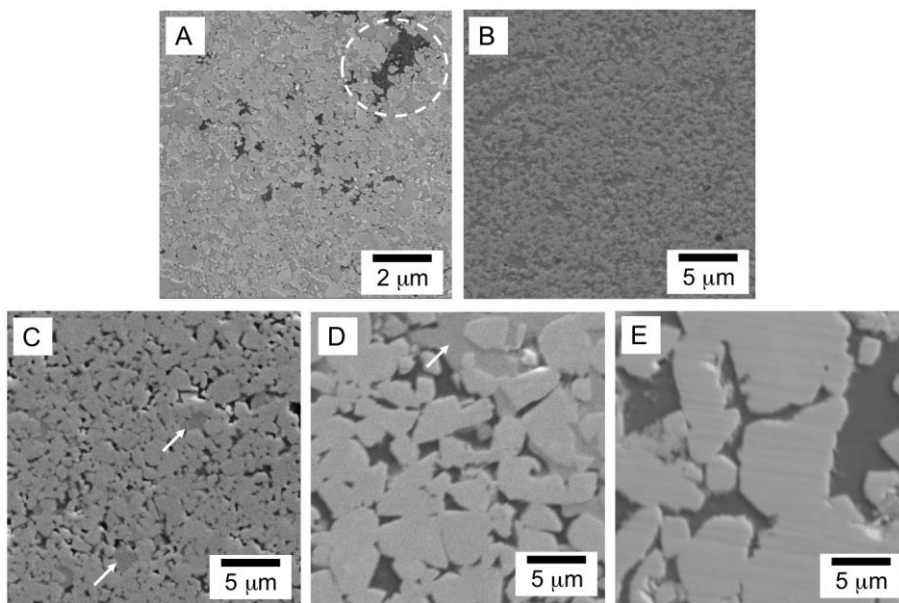

Figure 1: SEM of each sample used in this study (WC particle size classification in upper-left given in Table 1).
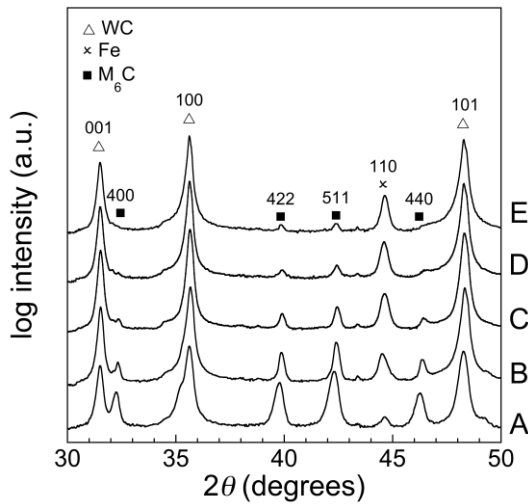
Figure 2:   XRD patterns showing progressive increase in Fe3W3C and decrease in FeCr as the grain size decreases from E to A. M = Fe, W.

Table 2:   Microstructural characteristics of WC-FeCr.

Grade	$<d_{WC}>$(μm)	σ_d (μm)	f_{M6C} (%)	f_{FeCr} (%)
A	0.21	0.11	31	2.1
B	0.35	0.15	7.5	6.7
C	0.78	0.46	2.5	8.3
D	2.4	1.3	1.4	9.7
E	5.4	3.3	1	9.1

These qualitative trends are quantified in Table 2, which gives the relative volume fractions of Fe_3W_3C and FeCr, denoted f_{M6C} and f_{FeCr} respectively. The volume fractions are taken from Rietveld refinement fits of the XRD data in Fig. 2. f_{M6C} increases from 1 % for the coarsest grained material (E), to about 31 % for the ultra-fine grained sample (A). f_{FeCr} on the other hand decreases from about 9 % to 2 % for the same samples. Table 2 also shows the mean and standard deviation in WC grain size, $<d_{WC}>$ and σ_d respectively, as extracted from the micrographs in Fig. 1. $<d_{WC}>$ varies from about 0.2 to 5 μm, while σ_d is consistently about 40–60 % of $<d_{WC}>$.

Thermal expansion

Fig. 3a shows raw thermal expansion curves for each sample from the cooling segment. Samples B-E have been offset in increments of 1×10^{-3} for clarity. There is a gradual increase in the gradient of the curves from about 6.5×10^{-6}/K at lower temperatures to about 8×10^{-6}/K at high temperatures. At 800-900 °C there is a discontinuous shrinkage in the samples, indicated by the markers below each curve, corresponding to the allotropic phase transformation in FeCr. These transformations are explored further in Fig. 4; for now we focus on the thermal expansion coefficients.
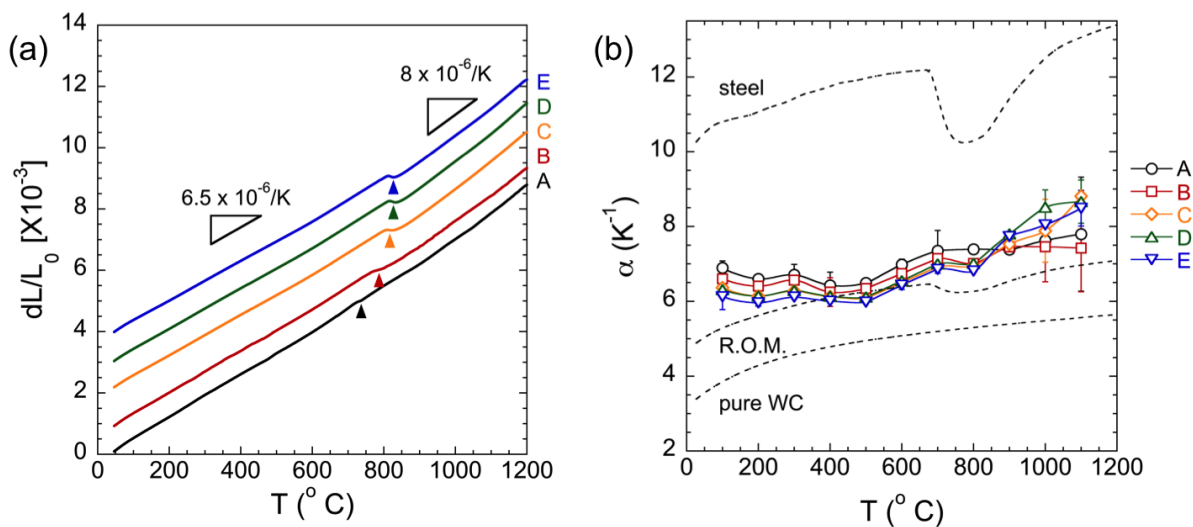
Figure 3:   (a) Raw thermal expansion curves showing the discontinuous shrinkage. (b) Physical thermal expansion coefficients as a function of temperature. The rule of mixtures model between pure WC and ferritic steel generally underestimates the experimental data. Error bars represent difference between heating and cooling segments.

The physical thermal expansion coefficients (α) are plotted in Fig. 3b. At low temperatures, α varies between about 6 and 7 x 10^{-6} K^{-1}, which is in relatively good agreement with previous reports of thermal expansion in WC-Co of between 5 and 6 x 10^{-6} K^{-1} [8]. Finer grained materials show larger α-coefficients, which is probably due to the presence of increased Fe_3W_3C. At higher temperatures α increases to between about 7 and 9 x 10^{-6} K^{-1} at 1100 °C. Overlayed on the plot are literature α-curves for a ferritic steel [17] and pure WC [18], shown in dotted lines. The rule of mixtures for a composite between the two at 10 wt.% WC is also shown. The model agrees well with the data in the range 400–600 °C but underestimates α outside this range.

The discontinuous shrinkage around 800–900 °C is explored in more detail in Fig. 4a, which shows a close up of the thermal expansion curves for sample D around the transformation event, under both heating and cooling. The primary axis of Fig. 4a shows the raw thermal expansion data, where the cooling curve has been off-set by 1 x 10^{-3} for clarity. The strain of the transformation is indicated by the symbols $\varepsilon_{T,h}$ and $\varepsilon_{T,c}$ for heating and cooling respectively. The secondary y-axis shows the corresponding differential of the thermal expansion curves, where the peak reveals the exact temperature of the phase transformation. On heating, the transition peak occurs at 915 °C and on cooling at 825 °C.

Figs. 4b and 4c show the transformation strains, ε_T, and transformation temperatures, T, plotted against WC grain size. The transformation temperatures lie either side of the BCC→FCC allotropic phase transformation temperature reported to be 855 °C in Fe-8 wt.% Cr [13]. For all samples there is clear transformation hysteresis – i.e. a difference in transition temperature between heating and cooling. The transition hysteresis appears to increase with decreasing WC grain size. Some of this hysteresis can be accounted for by the fact that the transition rate is governed by a diffusion controlled nucleation and growth mechanism [19]. Such hysteresis has been explicity observed in HT9 steel to be about 110 °C [20], which is comparable to the hysteresis seen here in the coarser-grained composites. Fig. 4b plots the corresponding transformation strain, ε_T. Since finer grained samples contained less BCC FeCr
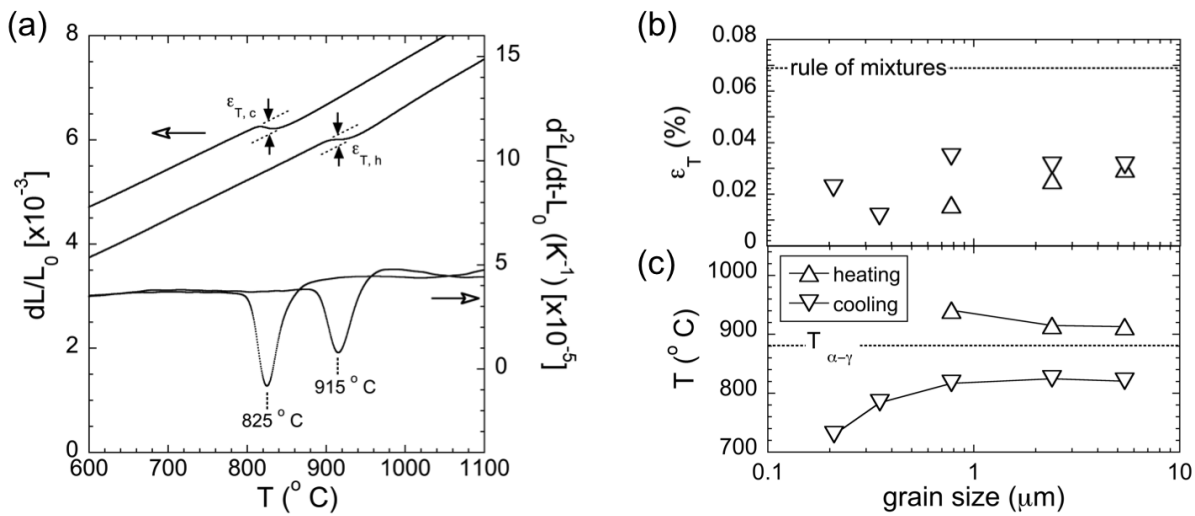
Figure 4:   (a) Expansion curve of sample D (primary y-axis) with its differential (secondary y-axis), showing a transformation hysteresis of ~ 90 °C. (b) The transformation strain, ε_T, shows a lower magnitude than would be predicted by a rule of mixtures (using data from [21]). (c) The transformation temperatures occur either side of the databook value for transformation in Fe-8 wt.% Cr [13] during heating and cooling. No heating peak is displayed for samples A and B as a clear peak was not observed.

phase, the strain reported has been normalised to the equivalent strain based on 10 wt.% FeCr phase. The average equivalent strain is between about 0.01 and 0.03 % which is significantly smaller than the predicted rule-of-mixtures linear shrinkage of 0.069 % (based on a volume change in pure Fe of 1.16 % [21]). The remainder of the volumetric strain is likely to be accommodated by strain in the WC phase; i.e. during heating, some of the shrinkage in the FeCr phase will be offset by a corresponding expansion in the surrounding WC phase.

Thermal diffusivity and specific heat

Fig. 5 shows the thermal diffusivity of all 5 grades of WC-FeCr hardmetal. The datasets have been fit by a simple power law expression:

$$\lambda = \lambda_{300K} \left(300/T\right)^{\beta} \tag{1}$$

where λ_{300K} is the room temperature diffusivity, T is the temperature, and β is a temperature dependency factor, wherby $\beta = 1$ indicates strong inverse temperature dependence and $\beta = 0$ indicates complete temperature-independence. The β values for each sample are indicated in parentheses in the legend.

We highlight three observations: Firstly, diffusivity increases dramatically with increasing WC grain size, with room temperature thermal diffiusivity varying from about 16 mm^2/s in the case of sample A, to 39 mm^2/s for sample E. Secondly, the diffusivity curves are much flatter (i.e. less temperature dependent) for the fine-grained materials. For example, samples A and E have β-exponents of 0.26 and 0.83 respectively. This tendency towards a flatter diffusivity profile is suggestive of an increased dominance in interfacial scattering, which is temperature-independent, in finer-grained structures. On the other hand, in coarser materials, it is likely that vibrational (i.e. phonon) scattering will dominate, which is highly temperature dependent. Such observations are consistent with measurements made by Frandsen and Williams on the WC-Co system [10], although their measurements were made at much lower
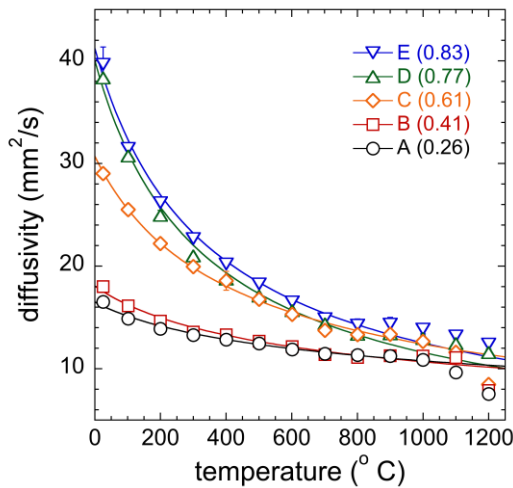
Figure 5:   Thermal diffusivity for samples of different WC grain size. Data has been fitted using Eq. 1. Error bars represent the standard deviation in 3 separate shots at each temperature.

temperatures, between 4 K and 300 K. Thirdly, the rapid decrease in diffusivity between 1100 and 1200 °C can be attributed to the formation of a liquid eutectic phase (at 1143 °C in WC-Fe [22])

Fig. 6 shows the specific heat capacity, C_p, of the B-grade and D-grade samples. In both samples there is an overall increase in specific heat with temperature, from about 0.21 J/g-K at 50 °C to about 0.29 J/g-K at 1000 °C. Plotted alongside these curves is data collected on an analogous WC-Co composite (with 9 wt.% binder) between about 100 and 700 °C, collected by Kny and Neumann [11]. Good agreement is shown between the WC-FeCr and WC-Co data, which is expected as the specific heats of Fe and Co are similar (0.449 and 0.421 J/g-K respectively at 298 K).

Above 700 °C there are three discontinous events in the specific heat signals:

- At 764 °C a peak in C_p occurs which coincides well with the predicted Curie transition temperature of 764 °C in Fe-8 wt.% Cr [13], i.e. where ferromagnetic materials lose their permanent magnetism;
- At about 850 °C (843 °C for sample D) another peak occurs, which is close to the allotropic phase transformation temperature of 855 °C [13]. The integrated peak intensity for sample D is about 2.3 J/g. If divided by the nominal mass fraction of FeCr (10 %) this equates to a heat of transformation of 23 J/g, which is close to the databook value for the enthalpy of transformation in pure Fe: $\Delta H_{\alpha\text{-}\gamma} = 18.1$ J/g [14];
- At 1170 °C there is a sharp transient associated with the formation of a liquid eutectic phase.
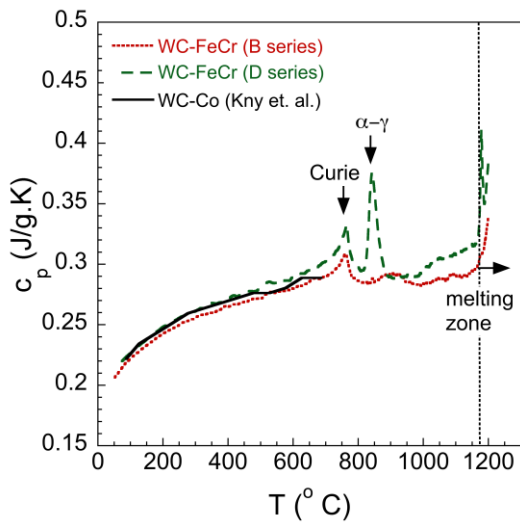
Figure 6: Specific heat of samples B and D, compared to literature data for an analagous WC-Co hardmetal [11].

Thermal conductivity

By combining data from the above measurements, thermal conductivity, κ, can be calculated using:

$$\kappa = \lambda \bullet \rho \bullet C_p \tag{2}$$

where λ, ρ and C_p are the thermal diffusivity, density and specific heat capacity respectively. Table 3 shows the thermal conductivity at 25 °C and at 600 °C, denoted $\kappa_{25\,C}$ and $\kappa_{600\,C}$, for each grade. To calculate κ, diffusivity is taken from Fig. 5; density values are taken from Table 1 (and corrected for thermal expansion from Fig. 3); and c_p is extracted from the average of the curves in Fig. 6.

Fig. 7 plots the thermal conductivity data from Table 3 against WC grain size. For comparison, data on standard WC-Co materials, reported at 25 °C by Perecherla and Willliams [9] and at 600 °C by Neumann and Kny [11], are shown in closed symbols. The high temperature WC-Co data was collected on samples with 9 wt.% binder and are thus directly comparable. However, the low temperature data from Perecherla and Willliams required some analysis since their samples had a range of binder contents from 1.5 to 30 wt.%. Therefore, linear fits were made to conductivity vs binder content plots at each measured WC grain size and the value corresponding to 10 wt.% binder was read-off and plotted in Fig. 7.

Table 3:   Thermophysical properties of WC-FeCr hardmetals.

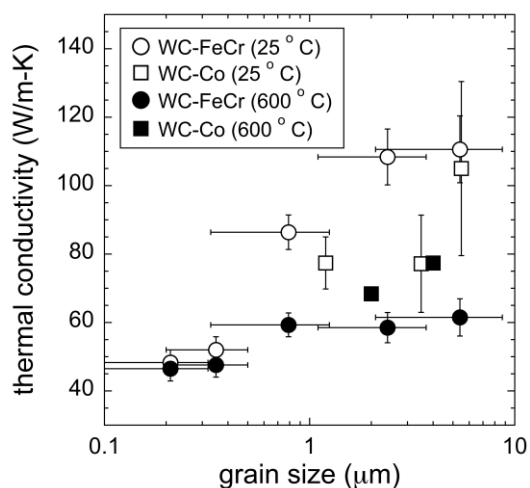| Grade	$\kappa_{25\,C}$ (W/m-K)	$\kappa_{600\,C}$ (W/m-K)
A	48	46
B	52	48
C	86	59
D	108	59
E	111	61

Figure 7:   Room temperature thermal conductivity for WC-10M hardmetals where M=Co (closed symbols) and Fe-8 wt.% Cr
(open). 10 wt.% binder was present in each case. FeCr-bound materials show a comparable values for thermal
conductivity to Co-bound materials. Error bars as follows: WC-FeCr y-axis is product of standard deviations in λ, ρ
and c_p; WC-FeCr x-axis is standard deviation in WC grain size (Table 2); WC-Co y-axis is standard deviation across
all samples reported at given WC grain size.

Fig. 7 shows that the WC-FeCr composites investigated here have a similar thermal conductivity to
conventional WC-Co materials. At 25 °C, WC-FeCr showed a slightly higher thermal conductivity than
Co-bound materials by Perecherla and Willliams [9], however at 600 °C WC-FeCr showed a slightly
lower value than those studied by Neumann and Kny [11]. The fact that FeCr-bound composites could
perform as well as Co-bound materials is unexpected since the room temperature thermal conductivity of
Co is greater than that of FeCr – i.e. 100 W/m-K for Co [23] vs. about 40 W/m-K for Fe-4.8 wt.% Cr [24].
We highlight three possible explanations for this unexpected result: Firstly, due to solubility of C and W in
the binder (typically on the order of 0.1 and 10 wt.% respectively for Co) there might be extensive point-
defect scattering, and therefore differences in conducitivity of the FeCr and Co binders would be reduced
significantly. Second, the presence of M_6C phase in the WC-FeCr composites, which was particularly
pronounced in the finer-grained samples, will have a significant effect on thermal transport. Thirdly,
different measurement techniques were employed between the two studies. We used laserflash
analysis, which is a direct measurement technique, while Perecherla and Williams used thermal
comparitor measurements, which require comparison to some material of known conductivity, and are
thus subject to increased error.

Conclusions

The key steady-state thermophysical properties of WC-FeCr composites were as follows: The linear
thermal expansion coefficients increased from about 6.5 x 10^{-6} K^{-1} at ambient temperature to about 8 x
10^{-6} K^{-1} at 1100 °C. Thermal expansion was in general larger than that predicted by theory, probably due
to the presence of Fe_3W_3C phase. Thermal conductivity tended to increase with increasing WC grain
size, as did the degree of temperature dependence. These trends are in general agreement with
previous studies in WC-Co at much lower temperatures. The absolute values of thermal conductivity
were also similar to previously reported values for WC-Co. They varied from about 50 to 110 W/m-K at
25 °C, and about 50 and 60 W/m-K at 600 °C. The low variation in conductivity with grain size at 600 °C

compared to 25 °C is attributed to the increasing predominance of vibrational scattering over grain boundary scattering with increasing temperature.

The allotropic phase transformation in the binder induced some transient phenomena that are unique to the FeCr binder system: The most important of these from the perspective of thermomechanical stability is the instantaneous volume change observed upon heating and cooling. There was a large hysteresis in the transition temperatures, that tended to increase with decreasing WC grain size. The magnitude of the transformation strain was about a third of that predicted by the rule of mixtures, suggesting that residual stress could be accumulating in the WC phase.

The high thermal conductivity values reported here compared to WC-Co materials suggest WC-FeCr is a suitable replacement for WC-Co in thermally demanding applications. However, further work is required to quantify the magnitude of any residual stress that is introduced by the the allotropic phase transformation in the binder – and its effect (if any) on mechanical integrity must be determined.

Acknowledgements

References

1. T.W. Penrice, Alternative binders for hard metals, J. Mater. Shap. Technol. 5 (1987) 35–39. doi:10.1007/BF0283368

2. V.A. Tracey, Nickel in hardmetals, Int. J. Refract. Met. Hard Mater. 11 (1992) 137–149. doi:10.1016/0263-4368(92)90056-8

3. Abstract for TR-581 - Cobalt Metal, (n.d.). https://ntp.niehs.nih.gov/results/pubs/longterm/reports/longterm/tr500580/listedreports/tr581/index.html (accessed January 9, 2017)

4. C.G. Windsor, J.G. Morgan, P.F. Buxton, Heat deposition into the superconducting central column of a spherical tokamak fusion plant, Nucl. Fusion. 55 (2015) 023014. doi:10.1088/0029-5515/55/2/023014

5. W.D. Schubert, M. Fugger, B. Wittmann, R. Useldinger, Aspects of sintering of cemented carbides with Fe-based binders, Int. J. Refract. Met. Hard Mater. 49 (2015) 110–123. doi:10.1016/j.ijrmhm.2014.07.028

6. B. Wittmann, W.-D. Schubert, B. Lux, WC grain growth and grain growth inhibition in nickel and iron binder hardmetals, Int. J. Refract. Met. Hard Mater. 20 (2002) 51–60. doi:10.1016/S0263-4368(01)00070-1

7. O.J. Ojo-Kupoluyi, S.M. Tahir, B.T.H.T. Baharudin, M.A.A. Hanim, M.S. Anuar, Mechanical properties of WC-based hardmetals bonded with iron alloys – a review, Mater. Sci. Technol. 0 (2016) 1–11. doi:10.1080/02670836.2016.1186929

8.   B. Roebuck, M. Gee, E. Bennett, T. (United K. National Physical Lab., Mechanical tests for hardmetals, (1999). http://www.opengrey.eu/item/display/10068/646991 (accessed January 6, 2017)

9.   A. Perecherla, W.S. Williams, Room-Temperature Thermal Conductivity of Cemented Transition-Metal Carbides, J. Am. Ceram. Soc. 71 (1988) 1130–1133. doi:10.1111/j.1151-2916.1988.tb05804.x

10. M.V. Frandsen, W.S. Williams, Thermal Conductivity and Electrical Resistivity of Cemented Transition-Metal Carbides at Low Temperatures, J. Am. Ceram. Soc. 74 (1991) 1411–1416. doi:10.1111/j.1151-2916.1991.tb04121.x

11. E. Kny, W. Neumann, Factors Influence the Temperature and Thermal Conductivity of WC–Co Hard Metals, 11 Th Int. Plansee Semin. 2 (1985) 659–678

12. W. Neumann, Thermal Diffusivity of Cemented Carbides, in: T. Ashworth, D.R. Smith (Eds.), Therm. Conduct. 18, Springer US, 1985: pp. 473–481. http://link.springer.com/chapter/10.1007/978-1-4684-4916-7_44 (accessed February 22, 2017)

13. W. Xiong, M. Selleby, Q. Chen, J. Odqvist, Y. Du, Phase Equilibria and Thermodynamic Properties in the Fe-Cr System, Crit. Rev. Solid State Mater. Sci. 35 (2010) 125–152. doi:10.1080/10408431003788472.

14. L. Byeong-Joo, Revision of thermodynamic descriptions of the Fe-Cr & Fe-Ni liquid phases, Calphad. 17 (1993) 251–268. doi:10.1016/0364-5916(93)90004-U

15. J.M. Marshall, A. Kusoffsky, Binder phase structure in fine and coarse WC–Co hard metals with Cr and V carbide additions, Int. J. Refract. Met. Hard Mater. 40 (2013) 27–35. doi:10.1016/j.ijrmhm.2013.04.001

16. R.D. Cowan, Pulse Method of Measuring Thermal Diffusivity at High Temperatures, J. Appl. Phys. 34 (1963) 926–927. doi:10.1063/1.1729564

17. Phox.at - Thermophysics and Thermokinetics, (n.d.). http://phox.at/Download.php (accessed February 16, 2017)

18. R.R. Reeber, K. Wang, Thermophysical Properties of α-Tungsten Carbide, J. Am. Ceram. Soc. 82 (1999) 129–135. doi:10.1111/j.1151-2916.1999.tb01732.x

19. A. Borgenstam, M. Hillert, Bainite in the light of rapid continuous cooling information, Metall. Mater. Trans. A. 27 (1996) 1501–1512. doi:10.1007/BF02649810

20. L. Leibowitz, R.A. Blomquist, Thermal conductivity and thermal expansion of stainless steels D9 and HT9, Int. J. Thermophys. 9 (1988) 873–883. doi:10.1007/BF00503252

21. G.W. Greenwood, R.H. Johnson, The Deformation of Metals Under Small Stresses During Phase Transformations, Proc. R. Soc. Lond. Ser. Math. Phys. Sci. 283 (1965) 403–422

22. C.M. Fernandes, A.M.R. Senos, Cemented carbide phase diagrams: a review, Int. J. Refract. Met. Hard Mater. 29 (2011) 405–418

23. W.M. Haynes, CRC handbook of chemistry and physics, CRC press, 2014. https://books.google.co.uk/books?hl=en&lr=&id=bNDMBQAAQBAJ&oi=fnd&pg=PP1&ots=H7ezsmoBWF&sig=Lt3Hu0byDuVW6e8T2koO9sJk5c8 (accessed January 9, 2017)

24. G. Neuer, 3.3.1.7 Fe-based alloys, in: O. Madelung, G.K. White (Eds.), Therm. Conduct. Pure Met. Alloys, Springer Berlin Heidelberg, 1991: pp. 220–229. http://link.springer.com/chapter/10.1007/10031435_35 (accessed January 16, 2017)